*Article*

# Finite Element Analysis of Zirconia Dental Implant

Luca Fiorillo [1,2,*], Dario Milone [3], Danilo D'Andrea [3], Dario Santonocito [3], Giacomo Risitano [3], Gabriele Cervino [1] and Marco Cicciù [1]

[1] Department of Biomedical and Dental Sciences, Morphological and Functional Images, University of Messina, 98100 Messina, Italy
[2] Multidisciplinary Department of Medical-Surgical and Odontostomatological Specialties, University of Campania "Luigi Vanvitelli", 80121 Naples, Italy
[3] Department of Engineering, University of Messina, 98100 Messina, Italy
*  Correspondence: lfiorillo@unime.it; Tel.: +39-0902216941

**Abstract:** Titanium dental implants have had new competitors in recent years, such as fixtures made of zirconia, which promise better aesthetics. The purpose of this study is to evaluate their mechanical performance in silico (Finite Element Analysis). The investigation was performed on a single tooth Patent™ Dental Implant (Zircon Medical®, Altendorf, Switzerland) in two configurations: without offset (Test I) and with offset (Test II, 1.5 mm within the cortical bone). The Patent Implant system consists of two components: the implant with integrated abutment and the fibreglass post. The components of the dental implants were tested using a compression load of 400 N along the implant axis. The results showed that the chewing load generates stress distribution on the bone, therefore, the offset configuration should be avoided.

**Keywords:** finite element analysis; dental implant; zirconia

## 1. Introduction

A dental implant (endosseous implant) is a surgical device used to functionally and aesthetically rehabilitate the loss or congenital lack of one or more teeth [1]. Dental implants allow oral rehabilitation through direct bone support, a biological process known as osseointegration, in the mandible and the maxilla. Dental implants can be used to support single prosthetic crowns or full arches. The most frequently used material is commercially pure titanium, forming an intimate bond with the bone. Zirconia is a widely used material in dentistry for the production of dental crowns and bridges. Prosthetic elements made of zirconia are increasingly manufactured using CAD/CAM technology [2]. In orthopaedics, zirconia is used for joint components such as in the hip and knee [3]. Dental implants in this study are entirely made of zirconium oxide and the prosthetic component is a fibreglass reinforced resin [4].

The finite element analysis (FEA) or finite element method (FEM) is a numerical technique to seek approximate mechanical features by partial differential equations reducing the latter to a system of algebraic equations [5]. The main feature of the finite element method is discretization through the creation of a grid (mesh) composed of primitives (finite elements) of the coded form (triangles and quadrilaterals for 2D domains, tetrahedra, and hexahedron for 3D domains). The solution of the hypothesis is assumed to be expressed by the linear combination of functions called basic functions or shape functions. Sometimes, the function is approximated, so the values that will provide the least error on the whole solution are considered [6,7]. The aim of this study is to evaluate the distribution of mechanical forces with the use of a Finite Element Analysis of implant and prosthodontic components in two offsets (0 mm and 1.5 mm within the cortical bone).

## 2. Materials and Methods

The study was performed on a single tooth "Patent™ Dental Implant" in two configurations: without offset (Test I, Figure 1a) and with offset (1.5 mm within the cortical bone, Test II, Figure 1b). The detailed geometry of the system, (for a gentle concession of the drawings) the boundary conditions and constraints, the material properties, and the load conditions were considered [6,8,9].
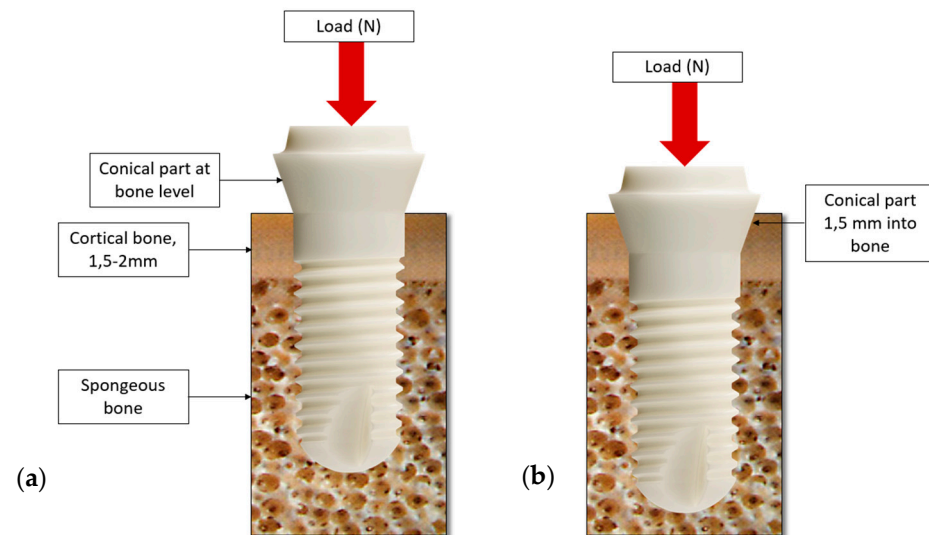


**Figure 1.** Two depth configurations of the implant conical part within the cortical bone: (**a**) without offset (Test I); (**b**) with 1.5 mm offset (Test II).

The modelling phase of the dental implant was performed using SpaceClaim® 2021 CAD software. The FEA (Finite Element Analysis) was performed in two phases: the finite element model construction phase and the processing of the results.

The FEA was performed with Ansys Workbench 2021R2® software. A linear static structural simulation was performed, evaluating the stress-strain relation between bone, dental implant, and post. A discretization method was assigned to all the elements of the geometry which consist of tetrahedral elements with a lower limit of 0.5 mm in size for the implant and 0.3 mm for the bone. A "MultiZone" meshing method was used with a Hexa mesh and SOLID186 elements, with a minimum size of 0.6 mm.

### 2.1. Materials

The Patent™ Implant system is "metal free"; the implant is made of zirconia ($Z_rO_2$) with an internal trilobate connection and the fibreglass reinforced resin post (Figures 2 and 3). This fibre post must be cemented with a dual resin cement.

The osseous portion of the implant has a threaded part and a 2 mm non-threaded part. The osseous portion has a surface roughness of approximately 7 µm, 4–5 times rougher than other commercially available titanium implants. The transgingival part of the implant has a machined surface that promotes soft tissue attachment.

The material's properties, Young's modulus ($E_{xx}$, $E_{yy}$, $E_{zz}$), Poisson's ratio ($v_{xx}$, $v_{yy}$, $v_{zz}$), tangential modulus ($G_{xx}$, $G_{yy}$, $G_{zz}$), and density ($\rho$), are referenced in [10–13]. The zirconia and the fibreglass reinforced resin were considered homogeneous and isotropic materials, whilst the bone tissues (cortical and cancellous), were considered orthotropic (Table 1).
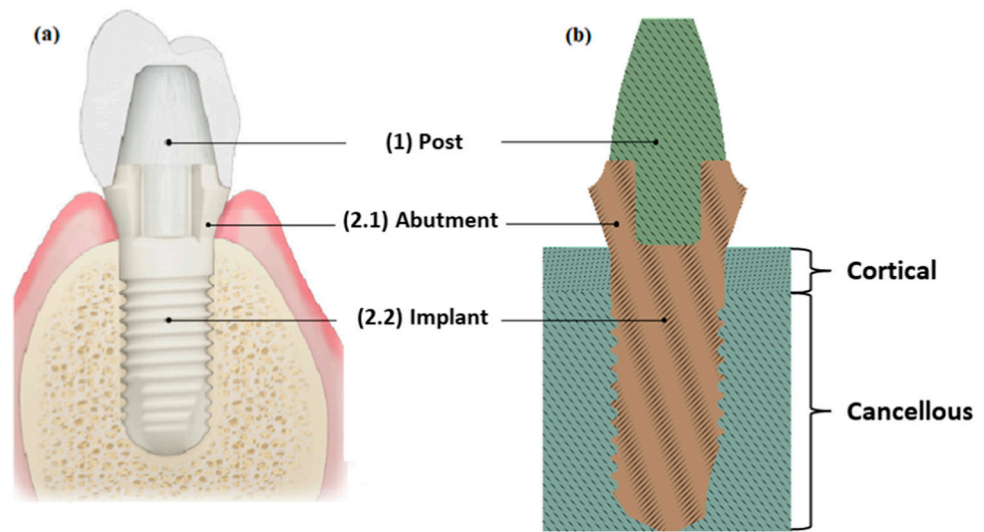
**Figure 2.** (**a**) Real configuration of the Patent™ Dental Implant and (**b**) reconstructed 3D CAD.
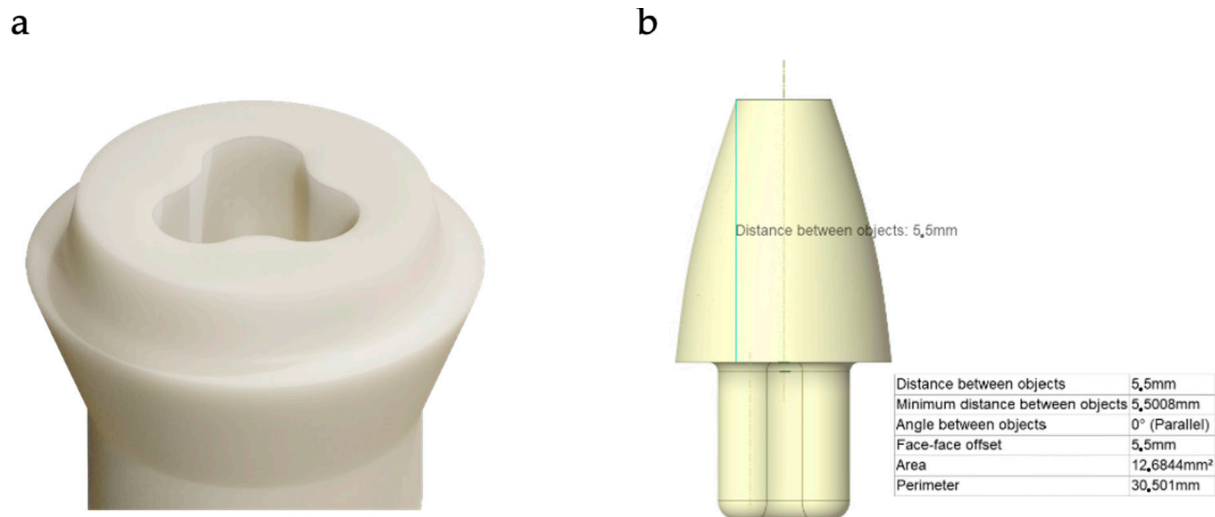


**Figure 3.** Dental implant connection detail (**a**) and fiber post detail (**b**).

**Table 1.** Material properties accordingly to the literature [1–4].

| Properties | Cortical Bone | Cancellous Bone | Zirconia ($Z_rO_2$) | Fibreglass Reinforced Resin |
|---|---|---|---|---|
| ρ (g/cm³) | 1.8 | 1.2 | | |
| $E_{xx}$ (GPa) | 9.6 | 0.144 | | |
| $E_{yy}$ (GPa) | 9.6 | 0.099 | 205 | 20 |
| $E_{zz}$ (GPa) | 17.8 | 0.344 | | |
| $v_{xx}$ | 0.55 | 0.23 | | |
| $v_{yy}$ | 0.30 | 0.11 | 0.3 | 0.22 |
| $v_{zz}$ | 0.30 | 0.13 | | |
| $G_{xx}$ (GPa) | 3.10 | 0.053 | | |
| $G_{yy}$ (GPa) | 3.51 | 0.063 | 78.846 | 8.1967 |
| $G_{zz}$ (GPa) | 3.51 | 0.045 | | |

*2.2. Boundary Conditions*

The prosthetic component is a post; this is cemented to the implant and the restoration is cemented over the post (see the upper part of the implant, Figure 1). The combination of the very stiff zirconia and the more flexible (Young's modulus similar to dentine) fibreglass post gives a very favourable load distribution of the masticatory forces.

The components of the dental implants were evaluated using a compression load of 400 N along the axial load (Y direction) [5]. To properly model the boundary conditions of the jaw bones, the medial sides (Figure 4) of the bone were fixed, while the buccal and lingual directions were free.
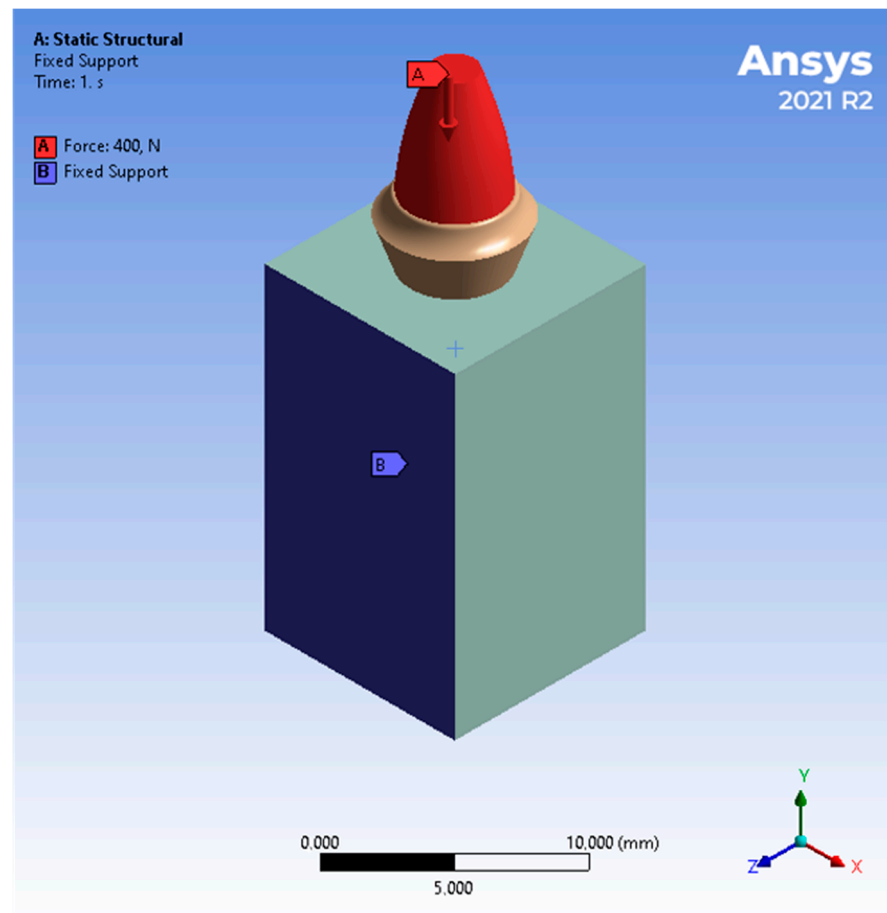


**Figure 4.** Boundary conditions of the FEA. The compressive force is applied on the post surface (red surface), and the constraints are applied on the front and rear sides of both cortical and cancellous bone (z-direction).

The bone-implant contact condition was modelled as a "frictional" contact system, with a friction coefficient of 0.15 [7] to simulate the osseointegration of the implant, allowing the transmission of a certain amount of shear stress. The contact between the cortical bone and the cancellous bone was set as "bonded". Furthermore, the contact between the post and the implant was modelled as "bonded" [14,15].

## 3. Results

An FEA (Finite Element Analysis) is applied to the simulation of the effects of stress on the implant and its surrounding bone [16,17].

Maximum stress values represent numerical singularities calculated by the software, they have been obscured (violet colour in the following figures), while minimum calculated

stresses have been obscured to highlight stresses due to chewing loads (grey colour in the following figures) (Figure 5).
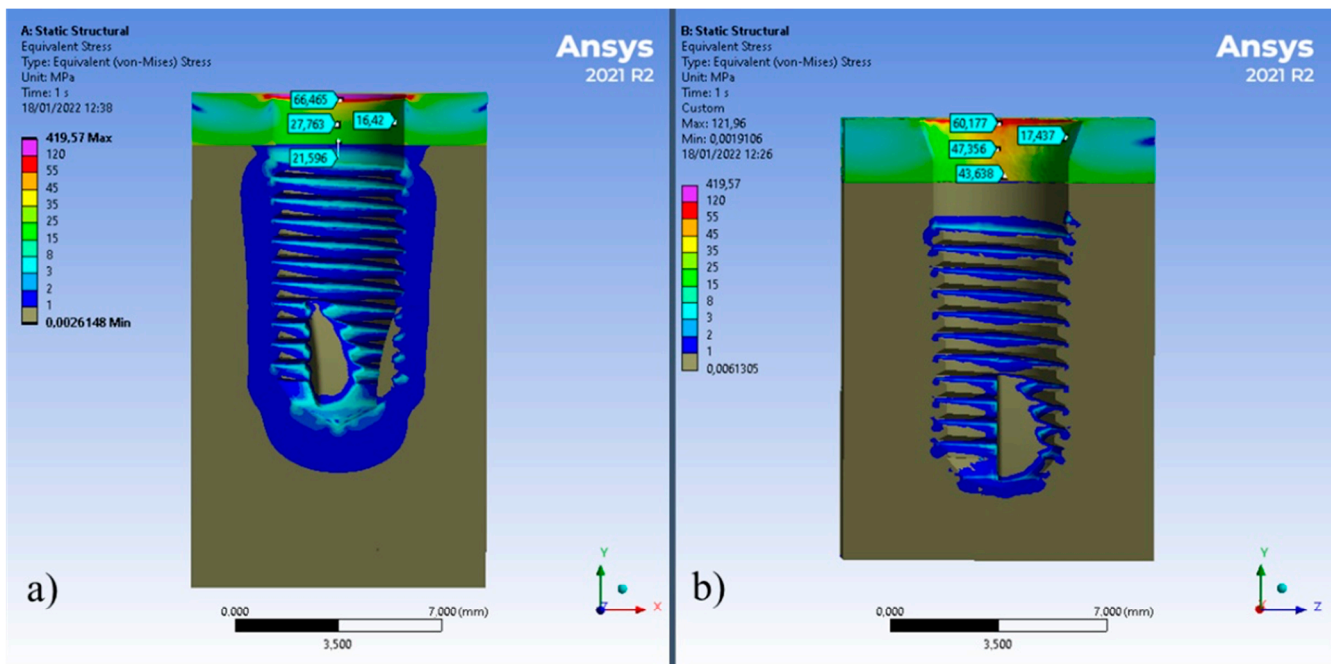


**Figure 5.** Stress distribution on cortical bone: (**a**) Test I and (**b**) Test II.

The stress distribution within the cortical bone is lower for Test I compared to Test II. The interfaces between cortical and cancellous bone were 48% higher in Test II than in Test I. The offset configuration (Test II) creates peak compressive stress within the cortical bone and is characterized by a large contact area (the abutment section of the prosthesis) of Test I. Figure 6 shows the cortical bone stress. Test I shows lower stress on the cortical and, excluding the purple points (points of singularity), with a homogeneous distribution in the periodontal area, with a clear decrease in stress along the thickness of the cortical. In Test II, shown in Figure 6b, stress on a portion of the periodontal area appears with a non-uniform distribution.
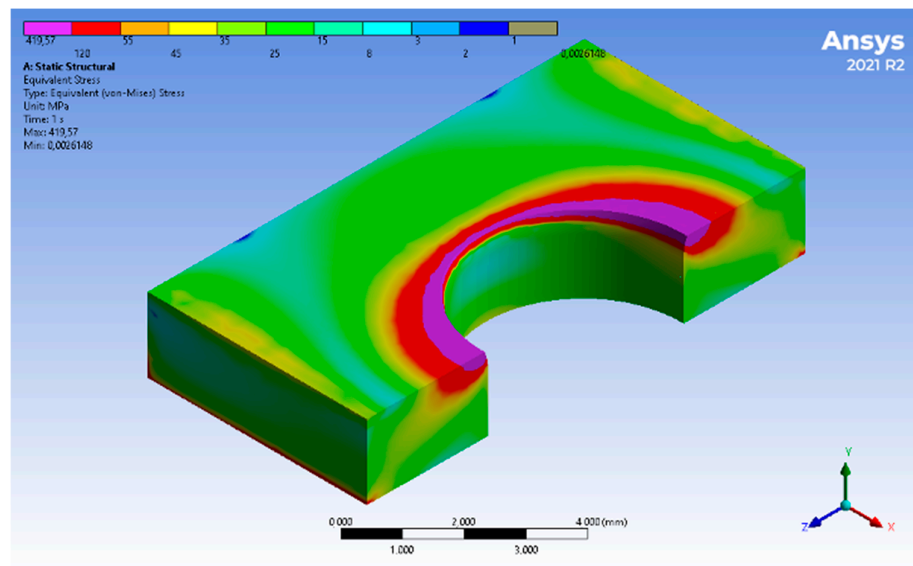
Figure 7 shows the stress distribution on the cancellous bone for Tests I and II. There is a difference of about 10 MPa on the first thread of the implant for Test I compared to Test II. At the bottom of the implant, the stress is 40% higher on Test I rather than Test II. The offset configuration decreases stress on the cancellous bone by compression on the cortical bone [18–20].

The longitudinal and axial stress paths were also analysed. Figure 8a shows the chosen axes.

Figure 9 shows the stress calculated for Test I along a horizontal path from the axis of the implant to the bone. Maximum stress is registered on the implant-bone interface. The value recorded at 2.5 mm from the bone prosthesis interface is 11% of the stress calculated on the interface.

Figure 10 shows the stress calculated for Test I along a vertical direction. Maximum stress appears on the prosthesis-bone interface. The value recorded at 2.5 mm from the bone prosthesis interface is equivalent to 14% of the stress calculated on the interface.

Figure 11 shows the stress calculated on Test II along a horizontal path. Maximum stress was registered on the prosthesis-bone interface. It follows an exponential curve with a negative coefficient. The value measured at 2.5 mm from the bone prosthesis interface is 87% of the stress calculated on the interface.

(**a**)
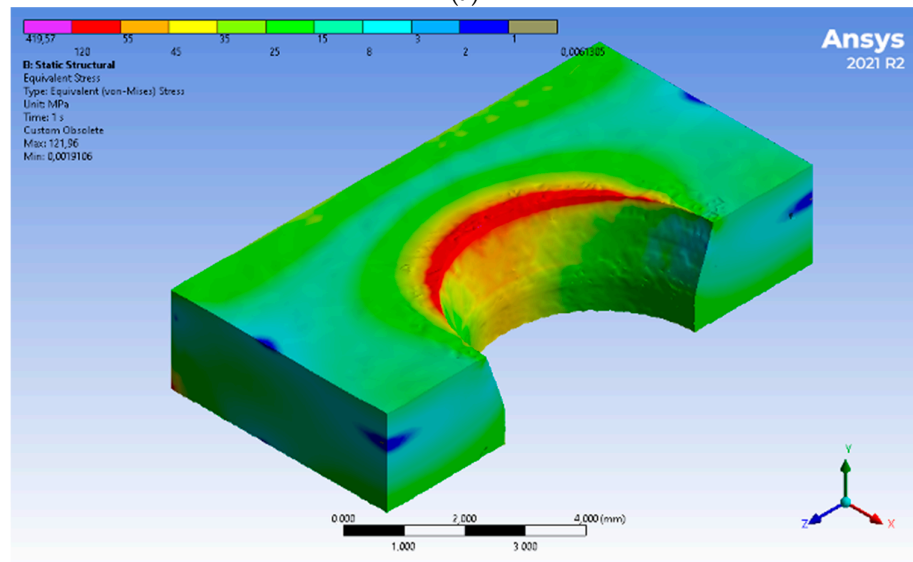


(**b**)

**Figure 6.** Stress distribution of the cortical bone in the isometric view: (**a**) Test I and (**b**) Test II.
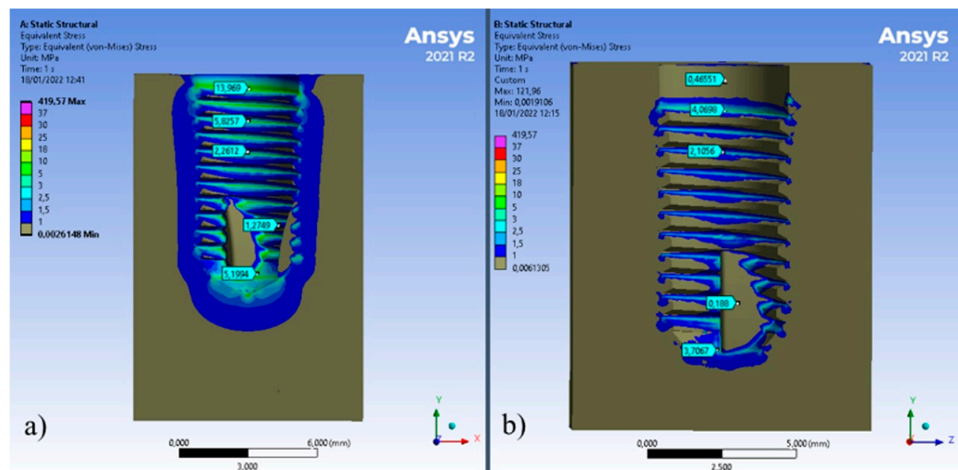


**Figure 7.** Stress distribution on cancellous bone: (**a**) Test I and (**b**) Test II.
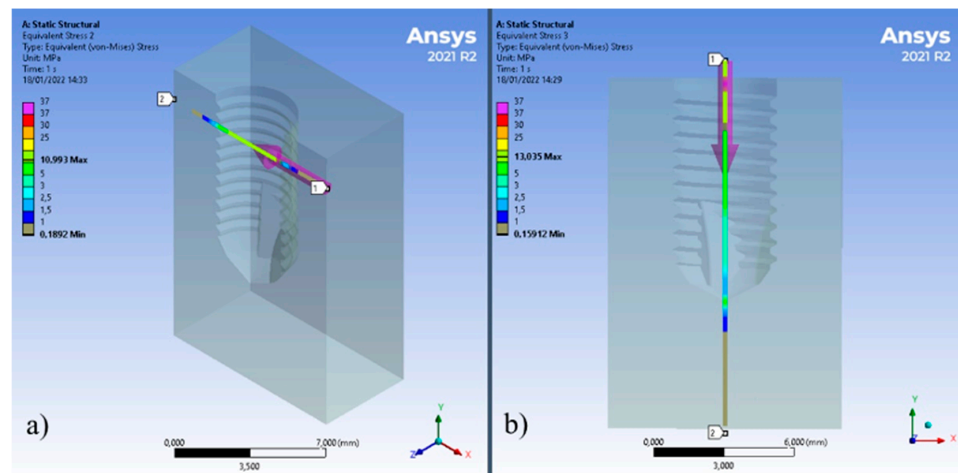
**Figure 8.** Stress path on cancellous bone: (**a**) longitudinal and (**b**) axial.
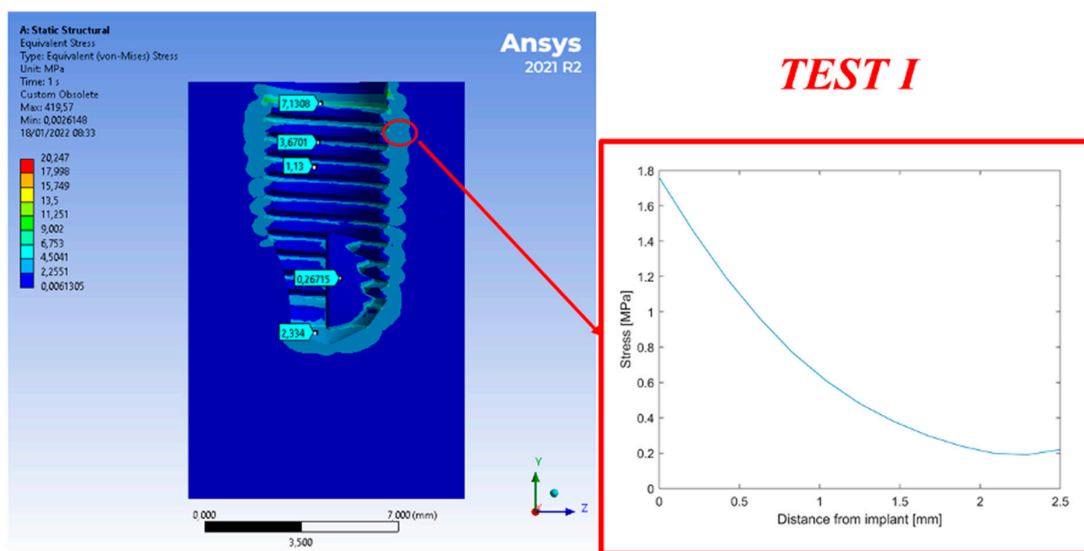
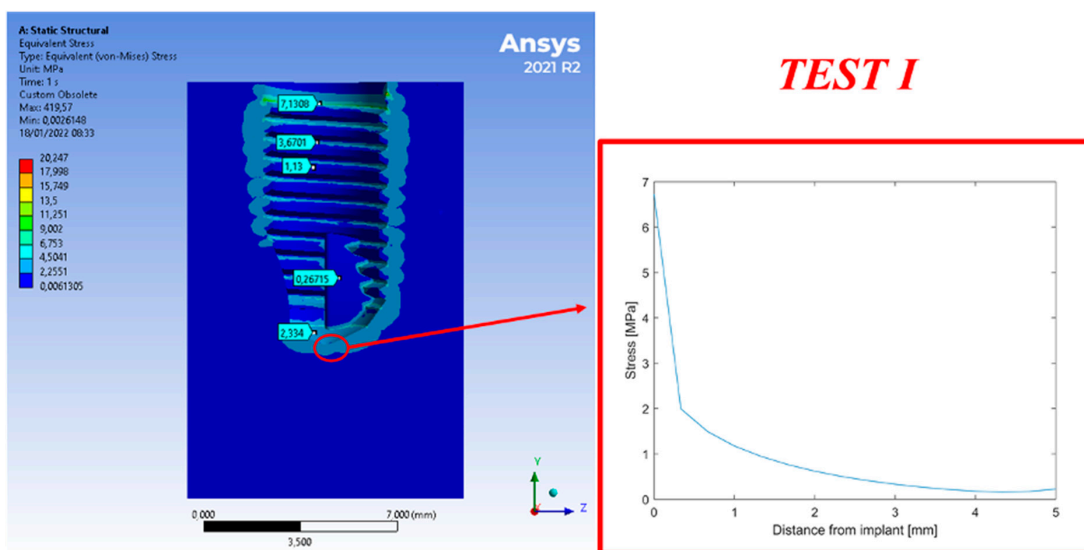

**Figure 9.** Horizontal stress path (Test I).



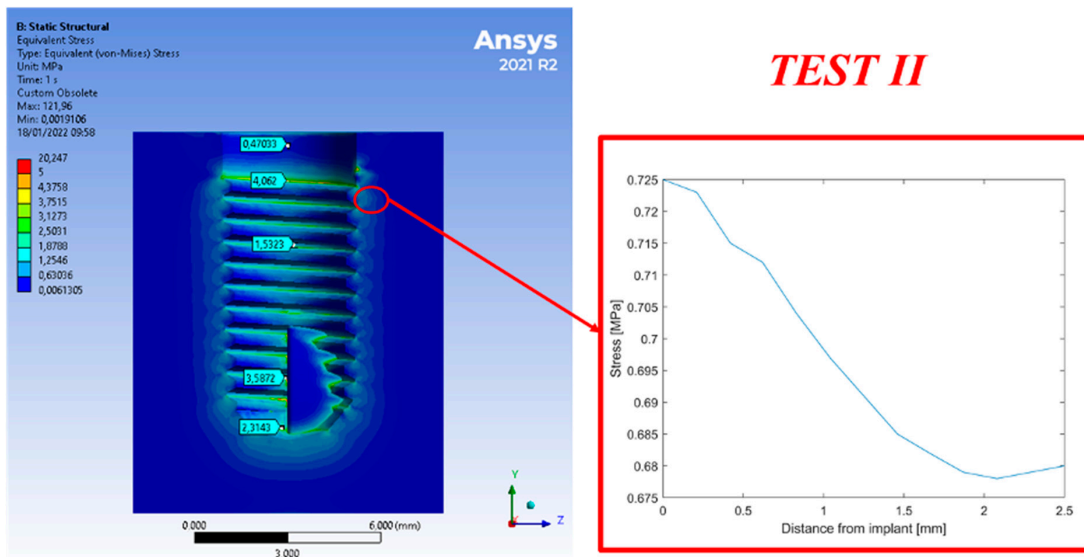**Figure 10.** Vertical stress path (Test I).

**Figure 11.** Horizontal stress path (Test II).

Figure 12 shows the stress calculated on Test II along a vertical path. Maximum stress is registered around the prosthesis/bone interface. This follows an exponential curve with a negative coefficient. The value recorded at 2.5 mm from the bone prosthesis interface is 29% of the stress calculated on the interface.
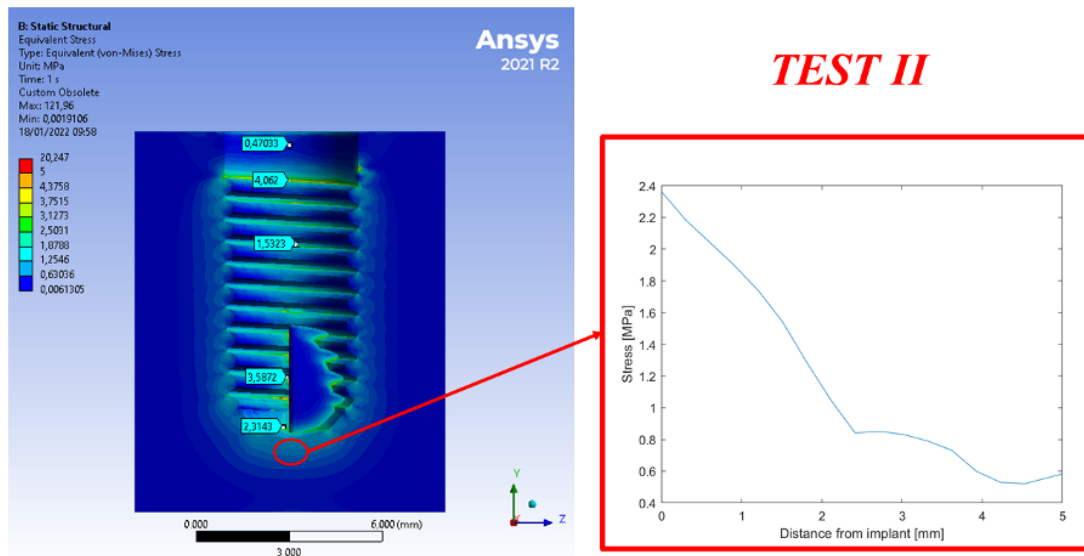


**Figure 12.** Vertical stress path (Test II).

## 4. Discussion

The titanium material, in its commercially pure form (CP4), is chosen for dental implants due to its mechanical strength and high biocompatibility [21–25]. Many dental implants have a textured surface (through milling, anodic oxidation, or various sandblasting methods) to increase their surface area and their potential for osseointegration. Despite this, titanium has a colour that could cause blemishes if the tissue undergoes resorption or if they are very thin. However, dental implants in zirconia have a white color.

In the biomechanical field, the tension distribution is analysed both in biological structures, to see how much the coupling with an artificial structure (e.g., prosthesis or implant) modifies the structural response to external stresses, and in artificial structures, to check their resistance capacity. The identification of the distribution of tensions in a structure is important as it highlights which areas are most stressed and at risk of rupture.

In the case of biological tissues, this includes necrosis, hypertrophy, and atrophy. In the analysis of the stress state of the biomechanical systems, particular attention was paid to the jaw cortical bone, as it was one of the most stressed parts, and the tension values in the areas of interface with the implant were compared, since experience indicates it as being the most affected by bone resorption. Other studies [8] on cancellous and cortical bone vary, depending on the implant geometry, between 4–13 MPa and 12–29 MPa, with the same chewing loads adopted in this study and the same values for the bone tissue.

Zirconia endosseous components, which are highly biocompatible and with high biomechanical performance, are used for the construction of orthopaedic prostheses [26,27]. They also have other favourable factors, such as less plaque formation and better aesthetics. However, from the first studies, it seems that the performance of this material from the point of view of resistance to disconnection (unscrewing) is lower than those obtainable with titanium, even if an adequate surface treatment could compensate for this problem [21,28,29].

Zirconia is affected by a low-temperature degradation process. This is due to a slow transformation from the metastable tetragonal to the monoclinic phase [30].

The implants under study showed excellent results in the simulation, there was no risk of fracture, neither of the abutment nor the implant. The simulation in [31] also showed a low-risk fracture connection relationship between the implant fixture and the abutment. Forces on the peri-implant are distributed in both simulations. In Test I with a supraperiosteal fixture, the forces that are discharged are higher [32]. Forces distributed unevenly on the peri-implant bone can be linked to peri-implant disease or to the time and physiological alteration of the jaws [33,34]. In summary, the different distribution of forces could aggravate bone health.

## 5. Conclusions

According to the data obtained from this study, Test I (zero offset) shows higher stress on the cancellous bone and lower on the cortical bone. The tested configurations generated stress on the bone close to yielding, however, the offset configuration (Test I) has better results than Test II to generate lower compressive stress on the cortical bone and higher stress on the cancellous bone.

## References

1. Gordon, L.M.; Cohen, M.J.; MacRenaris, K.W.; Pasteris, J.D.; Seda, T.; Joester, D. Dental materials. Amorphous intergranular phases control the properties of rodent tooth enamel. *Science* **2015**, *347*, 746–750. [CrossRef] [PubMed]
2. Lavorgna, L.; Cervino, G.; Fiorillo, L.; Di Leo, G.; Troiano, G.; Ortensi, M.; Galantucci, L.; Cicciù, M. Reliability of a virtual prosthodontic project realized through a 2d and 3d photographic acquisition: An experimental study on the accuracy of different digital systems. *Int. J. Environ. Res. Public Health* **2019**, *16*, 5139. [CrossRef]
3. Baun, W.L. Phase Transformation at High Temperatures in Hafnia and Zirconia. *Science* **1963**, *140*, 1330–1331. [CrossRef] [PubMed]
4. Roehling, S.; Schlegel, K.A.; Woelfler, H.; Gahlert, M. Zirconia compared to titanium dental implants in preclinical studies-A systematic review and meta-analysis. *Clin. Oral Implant. Res.* **2019**, *30*, 365–395. [CrossRef] [PubMed]
5. Kolata, G.B. The finite element method: A mathematical revival. *Science* **1974**, *184*, 887–889. [CrossRef] [PubMed]

6.  Crimi, S.; Defila, L.; Nanni, M.; Cicciù, M.; Fiorillo, L.; Cervino, G.; Marchetti, C.; Bianchi, A. Three-Dimensional Evaluation on Cortical Bone During Orthodontic Surgical Treatment. *J. Craniofacial Surg.* **2020**, *31*, 1637–1646. [CrossRef]

7.  D'Andrea, D.; Pistone, A.; Risitano, G.; Santonocito, D.; Scappaticci, L.; Alberti, F. Tribological characterization of a hip prosthesis in Si3N4-TiN ceramic composite made with Electrical Discharge Machining (EDM). *Procedia Struct. Integr.* **2021**, *33*, 469–481. [CrossRef]

8.  Fiorillo, L.; Cicciù, M.; D'Amico, C.; Mauceri, R.; Oteri, G.; Cervino, G. Finite Element Method and Von Mises Investigation on Bone Response to Dynamic Stress with a Novel Conical Dental Implant Connection. *BioMed Res. Int.* **2020**, *2020*, 2976067. [CrossRef]

9.  Cicciù, M.; Cervino, G.; Terranova, A.; Risitano, G.; Raffaele, M.; Cucinotta, F.; Santonocito, D.; Fiorillo, L. Prosthetic and Mechanical Parameters of the Facial Bone under the Load of Different Dental Implant Shapes: A Parametric Study. *Prosthesis* **2019**, *1*, 41–53. [CrossRef]

10. Zhang, Y.; Lawn, B.R. Evaluating dental zirconia. *Dent. Mater.* **2019**, *35*, 15–23. [CrossRef]

11. Zhang, Y.; Lawn, B.R. Novel Zirconia Materials in Dentistry. *J. Dent. Res.* **2018**, *97*, 140–147. [CrossRef] [PubMed]

12. Hanawa, T. Zirconia versus titanium in dentistry: A review. *Dent. Mater. J.* **2020**, *39*, 24–36. [CrossRef] [PubMed]

13. Filardi, V. Stress shielding FE analysis on the temporomandibular joint. *J. Orthop.* **2020**, *18*, 63–68. [CrossRef]

14. Marcián, P.; Borák, L.; Valášek, J.; Kaiser, J.; Florian, Z.; Wolff, J. Finite element analysis of dental implant loading on atrophic and non-atrophic cancellous and cortical mandibular bone—A feasibility study. *J. Biomech.* **2014**, *47*, 3830–3836. [CrossRef]

15. Crespi, R.; Capparé, P.; Romanos, G.E.; Mariani, E.; Benasciutti, E.; Gherlone, E. Corticocancellous porcine bone in the healing of human extraction sockets: Combining histomorphometry with osteoblast gene expression profiles in vivo. *Int. J. Oral Maxillofac. Implant.* **2011**, *26*, 866–872.

16. Macedo, J.P.; Pereira, J.; Faria, J.; Pereira, C.A.; Alves, J.L.; Henriques, B.; Souza, J.C.M.; López-López, J. Finite element analysis of stress extent at peri-implant bone surrounding external hexagon or Morse taper implants. *J. Mech. Behav. Biomed. Mater.* **2017**, *71*, 441–447. [CrossRef]

17. Clift, S.E.; Fisher, J.; Watson, C.J. Finite element stress and strain analysis of the bone surrounding a dental implant: Effect of variations in bone modulus. *Proc. Inst. Mech. Eng. Part H* **1992**, *206*, 233–241. [CrossRef]

18. Soto-Penaloza, D.; Caneva, M.; Vina-Almunia, J.; Martin-de-Llano, J.J.; Penarrocha-Oltra, D.; Penarrocha-Diago, M. Bone-Healing Pattern on the Surface of Titanium Implants at Cortical and Marrow Compartments in Two Topographic Sites: An Experimental Study in Rabbits. *Materials* **2018**, *12*, 85. [CrossRef]

19. Lakes, R.S.; Katz, J.L.; Sternstein, S.S. Viscoelastic properties of wet cortical bone—I. Torsional and biaxial studies. *J. Biomech.* **1979**, *12*, 657–678. [CrossRef]

20. Brown, C.U.; Norman, T.L.; Kish, V.L., 3rd; Gruen, T.A.; Blaha, J.D. Time-dependent circumferential deformation of cortical bone upon internal radial loading. *J. Biomech. Eng.* **2002**, *124*, 456–461. [CrossRef]

21. Nicholson, W.J. Titanium Alloys for Dental Implants: A Review. *Prosthesis* **2020**, *2*, 100–116. [CrossRef]

22. Fiorillo, L.; Cicciù, M.; Tozum, T.F.; Saccucci, M.; Orlando, C.; Romano, G.L.; D'Amico, C.; Cervino, G. Endosseous Dental Implant Materials and Clinical Outcomes of Different Alloys: A Systematic Review. *Materials* **2022**, *15*, 1979. [CrossRef] [PubMed]

23. Fiorillo, L.; D'Amico, C.; Campagna, P.; Terranova, A.; Militi, A. Dental Materials Implant Alloys: An X-Ray Fluorescence Analysis On Fds76®. *Minerva Stomatol.* **2021**, *70*, 370–376. [CrossRef] [PubMed]

24. Chang, J.Z.; Tsai, P.I.; Kuo, M.Y.; Sun, J.S.; Chen, S.Y.; Shen, H.H. Augmentation of DMLS Biomimetic Dental Implants with Weight-Bearing Strut to Balance of Biologic and Mechanical Demands: From Bench to Animal. *Materials* **2019**, *12*, 164. [CrossRef]

25. Tallarico, M.; Meloni, S.M.; Park, C.-J.; Zadrożny, Ł.; Scrascia, R.; Cicciù, M. Implant Fracture: A Narrative Literature Review. *Prosthesis* **2021**, *3*, 267–279. [CrossRef]

26. Koller, M.; Steyer, E.; Theisen, K.; Stagnell, S.; Jakse, N.; Payer, M. Two-piece zirconia versus titanium implants after 80 months: Clinical outcomes from a prospective randomized pilot trial. *Clin. Oral Implant. Res.* **2020**, *31*, 388–396. [CrossRef]

27. Barazanchi, A.; Li, K.C.; Al-Amleh, B.; Lyons, K.; Waddell, J.N. Mechanical Properties of Laser-Sintered 3D-Printed Cobalt Chromium and Soft-Milled Cobalt Chromium. *Prosthesis* **2020**, *2*, 313–320. [CrossRef]

28. Petrović, Ž.; Šarić, A.; Despotović, I.; Katić, J.; Peter, R.; Petravić, M.; Petković, M. A New Insight into Coating's Formation Mechanism Between TiO2 and Alendronate on Titanium Dental Implant. *Materials* **2020**, *13*, 3220. [CrossRef]

29. Dong, H.; Liu, H.; Zhou, N.; Li, Q.; Yang, G.; Chen, L.; Mou, Y. Surface Modified Techniques and Emerging Functional Coating of Dental Implants. *Coatings* **2020**, *10*, 1012. [CrossRef]

30. Kohorst, P.; Borchers, L.; Strempel, J.; Stiesch, M.; Hassel, T.; Bach, F.-W.; Hübsch, C. Low-temperature degradation of different zirconia ceramics for dental applications. *Acta Biomater.* **2012**, *8*, 1213–1220. [CrossRef]

31. Pirjamalineisiani, A.; Sarafbidabad, M.; Jamshidi, N.; Esfahani, F.A. Finite element analysis of post dental implant fixation in drilled mandible sites. *Comput. Biol. Med.* **2017**, *81*, 159–166. [CrossRef] [PubMed]

32. Uccioli, U.; Fonzar, A.; Lanzuolo, S.; Meloni, S.M.; Lumbau, A.I.; Cicciù, M.; Tallarico, M. Tissue Recession around a Dental Implant in Anterior Maxilla: How to Manage Soft Tissue When Things Go Wrong? *Prosthesis* **2021**, *3*, 209–220. [CrossRef]

33. Shemtov-Yona, K.; Rittel, D. Fatigue of Dental Implants: Facts and Fallacies. *Dent. J.* **2016**, *4*, 16. [CrossRef] [PubMed]

34. Meijer, H.J.; Kuiper, J.H.; Starmans, F.J.; Bosman, F. Stress distribution around dental implants: Influence of superstructure, length of implants, and height of mandible. *J. Prosthet. Dent.* **1992**, *68*, 96–102. [CrossRef]